RESEARCH ARTICLE

# Application of a simple unstructured kinetic and cost of goods models to support T-cell therapy manufacture

Maryam Shariatzadeh[1] ⬤ | Adriana G. Lopes[2] | Katie E. Glen[1] | Andrew Sinclair[2] | Rob J. Thomas[1]

[1]Centre for Biological Engineering, Wolfson School of Mechanical and Electrical and Manufacturing Engineering, Loughborough University, Epinal Way, Loughborough University, Loughborough, UK

[2]Biopharm Services, Chesham, UK

**Correspondence**
Maryam Shariatzadeh, Centre for Biological Engineering, Wolfson School of Mechanical, Electrical and Manufacturing Engineering, Loughborough University, Epinal Way, Loughborough University, Loughborough, Leicestershire, LE11 3TU, UK.
Email: m.m.shariatzadeh@lboro.ac.uk

## Abstract

Manufacturing of cell therapy products requires sufficient understanding of the cell culture variables and associated mechanisms for adequate control and risk analysis. The aim of this study was to apply an unstructured ordinary differential equation-based model for prediction of T-cell bioprocess outcomes as a function of process input parameters. A series of models were developed to represent the growth of T-cells as a function of time, culture volumes, cell densities, and glucose concentration using data from the Ambr®15 stirred bioreactor system. The models were sufficiently representative of the process to predict the glucose and volume provision required to maintain cell growth rate and quantitatively defined the relationship between glucose concentration, cell growth rate, and glucose utilization rate. The models demonstrated that although glucose is a limiting factor in batch supplied medium, a delivery rate of glucose at significantly less than the maximal specific consumption rate ($0.05$ mg $1 \times 10^6$ cell h$^{-1}$) will adequately sustain cell growth due to a lower glucose Monod constant determining glucose consumption rate relative to the glucose Monod constant determining cell growth rate. The resultant volume and exchange requirements were used as inputs to an operational BioSolve cost model to suggest a cost-effective T-cell manufacturing process with minimum cost of goods per million cells produced and optimal volumetric productivity in a manufacturing settings. These findings highlight the potential of a simple unstructured model of T-cell growth in a stirred tank system to provide a framework for control and optimization of bioprocesses for manufacture.

**KEYWORDS**
cost analysis, modeling framework, process optimization, scalable T-cell manufacturing, T-cell processing

## 1 | INTRODUCTION

The launch of CAR-T cell therapy products including Kymriah and Yescarta are the first in a significant pipeline of T-cell based therapeutic products.[1,2] Such cell-based immunotherapies are set to change the treatment options for a range of previously hard to treat or fatal hematological malignancies.[3,4] However, as a new therapeutic class based on a relatively unexplored bioprocess input material,

primary T-cells manufacturing technology is particularly immature.[3] The knowledge of process control and its impacts on product quality, such as population distributions and yield, are significantly understudied relative to more established biopharmaceuticals.[5] This lack of knowledge restricts the opportunity for operational optimization that might drive down costs and/or create more consistent product.[6] Recent work in manufacturing processes has shown amenability to suspension scaled production and described some of the changes in the environment.[7] However, these descriptions fall short of providing the level of process understanding required for risk assessment of process deviations or selection of optimal process operation.[8,9] For example, given process constraints, such as a restricted bioreactor volume, the optimal medium exchange or concentrated batch feed strategy and the risk of any associated control deviations.[10,11]

The current manufacturing process for CAR-Ts uncovers how a cellular therapy with a complex manufacturing process has been successfully scaled out, streamlined, and optimized to ensure supply of the high-quality T-cell product to the global market.[9]

The CAR-T cell therapy manufacturing process begins by collecting the nonmobilized peripheral blood mononuclear cells (PBMC) from a patient through leukapheresis.[10] The leukaphereshed PBMC is cryopreserved within 24 h after collection at $-120°C$ for further processing. Dependent upon the patient's need PBMCs are then thawed under controlled conditions, followed by cell washing and T-cells selection and enrichment. T-cells are activated using CD3/CD28 antibody-coated paramagnetic beads before a transduction step using viral vectors. Following transduction and removal of excess vector and other residuals the cells are expanded in static cultures and then in bioreactors.[8,12] Cell expansion continues ex vivo until sufficient number of cells that meet the final product dose requirements have been achieved. To harvest the cells, the CAR-Ts are isolated from the beads, washed, and formulated in infusible media. The critical quality attributes of cells are evaluated to determine multiple parameters including: appearance, identity, safety, purity, potency, and quality of the final product.

During the industrial manufacturing of CAR-Ts for global clinical trial applications, multiple steps were taken to improve process performance and robustness and to maintain the quality of the product. The key process changes included: enhancement of process control to ensure product consistency, introducing the automation process and closed systems to ensure reproducibility while preventing the risk of contamination. Further validation of analytical methods was also applied to improve the consistency of the final product.[13]

T-cell based immunotherapy will require a consistent quality product in a suitable bioprocess format for manufacturing at scale. In order to ensure and maintain the quality of clinically relevant T-cell populations, a variety of quality control (QC) panel tests have been carried out by manufacturers to evaluate the expression levels of multiple T-cell surface antibodies including: $CD4^+/CD8^+$, CD45, and CCR7.[14,15] The presence or absence of these phenotypic markers will determine the diversity of T-cell subpopulations hence mandate the process condition including: feeding composition and rates to achieve targeted sub populations of T-cells that can be clinically relevant. For example, Naive T-cells are $CD45RA^+$, $CD45RO^-$, $CD62L^+$, and $CCR-7^+$. These markers change to $CD45RA'$, $CCR-7'$ in $CD8^+$ TEM cells. Thus, based on the expression level of these and other phenotypic markers T-cell subsets and subpopulations can be sorted, expanded, and analyzed for functional activities during immune responses against pathogenic agents or CAR-T cell therapies.[16,17]

The ongoing, continuous process improvements will result in further enrichment in the manufacturing of CAR-Ts including reduction in the throughput time from receipt of leukapheresis material to patient bedside.[8] One example of process improvement was demonstrated by the collaborative study conducted by National Cancer Institute and Kite Pharma, a Gilead company which underlined the significant correlation between the functionality of an anti-CD19 CAR-T-cell product before treatment, polyfunctional strength index, and response in non-Hodgkin lymphoma patients. Their findings show a high potential to predict the cancer patients objective response to CAR-T cell therapy before treatment, while highlighting the improvement achieved both in preinfusion product potency testing and cell product optimization.[4]

In common with all therapeutics, the industry standard for process development is a risk-based approach driven by robust experimental data.[16] Mathematical models that describe process outcomes in terms of process control variables are at the heart of such an approach.[17] They can support quantitative estimates of risk based on simulations of operating variation, either via methods such as the Monte-Carlo analysis of model parameters or control variable distributions, or extrapolation/interpolation to assess alternative operating conditions. Diverse outcomes will develop from variation in input cells and reagent indicating that process is highly dependent on process operation and specific autocrine and paracrine responses of T-cell subsets and sub populations.[16,17] Applying mathematical modeling, therefore, is a cost-effective approach that untangle, and control T-cells bioprocesses by predicting variability in process outcomes with respect to input variability thus identify process operation with acceptable risk and opportunities for process optimization.

Independent modeling approaches have previously been developed to provide a framework for bioprocess optimization of cell therapy manufacturing (Advanced Bioprocess Design, UK),[17,18] and, separately, the cost analysis of cell therapy manufacture (BioSolve, Biopharm Services, UK).[19,20] The bioprocess optimization is based on an ordinary differential equation approach to describe key process mechanisms in a low parameter (and generally unstructured) form that directly relate to process operation. The application of this framework in providing insight to T-cell manufacturing process optimization is reported in this article. The aim of this study was to describe how this modeling approach can be applied, with limited process data, to define medium exchange process operation limits in a stirred tank culture format. Therefore, to show how the approach can be evolved to provide further process insight as more analytical data, such as nutrient concentrations, becomes available. Gaining these insights will further assist in evaluation of the process optimization and risk understanding in cell therapy applications.

The second modeling approach was to use BioSolve commercial software as an independent model to provide an insight into the cost impact of defined optimized T-cell process choices and scale-up. Previous work in this area focused on cell therapy manufacturing processing platforms that relied on scale-out.[19,20] Most autologous cell therapies will require low-batch volumes, typically less than 5 L and hence do not take advantage of economies of scale. The smaller volumes, the larger number of batches and the variability of starting and finished cell materials pose a challenge to current processing platforms that rely on unscalable processing platforms.[21] Using scalable technologies would provide maximum flexibility, control, and monitoring in the cell culture platform to accommodate for the heterogeneity in the type and number of cells available initially from the patient.[22] Using modeling approaches such as the ones shown in this article would enable a preliminary analysis of the optimal way to process cells for a given starting cell number, best feeding strategy, and cost impact, before any experimentation or processing is undertaken. With further data, such a model could also indicate how cell growth can be sustained while selectively affecting the growth of specific sub-population of T-cells, hence would be highly applicable in T-cell/ CAR-T cell therapy manufacturing processes.[22]

## 2 | MATERIALS AND METHODS

### 2.1 | CD3$^+$/CD28$^+$ cell culture

Frozen PBMC vials were supplied by the Axol Bioscience (Cambridge, UK) with informed consent and national research ethics committee (NREC) ethical approval. Following the thaw of PBMC vial, CD3$^+$/CD28$^+$ T-cells were isolated and activated via positive selection using Dynabeads$^®$ human T-activator CD3$^+$/CD28$^+$ antibody labeled microbeads with ratio of 3:1 dynabeads per cells according to the manufacturer's instructions (Gibco™ by Life Technologies, UK). The activated T-cells were then inoculated at a density of $1 \times 10^6$ cells ml$^{-1}$ in RPMI (Thermofisher, UK) supplemented with 10% (v/v) Fetal Bovine Serum, Heat Inactivated, US origin Gibco (Fisher Science, UK), 1% (v/v) L-Glutamine (200 mM) (Thermofisher, UK) and 100 IU Human IL-2 IS (Miltenyi Biotec, DE).

Cells were cultured in T25 tissue culture flasks in humidified atmospheric O$_2$ and 5% CO$_2$ conditions at 37°C (5% CO$_2$ in air) for 7 days prior to bioreactor culture; they were fed daily from day 2 of culture by addition of 5 ml fresh medium. On day 7, dynabeads were removed from cells, cells were centrifuged at 300$g$ for 10 min and were re stimulated by addition of fresh dynabeads with ratio of 1:1. Cells were seeded in the Ambr$^®$15 bioreactor system (Sartorius Stedim, DE); nonsparged vessels were preconditioned as described previously,[23] and temperature, impeller speed, pH, and DO were set to 37°C, 450 RPM, pH 7.3, and 100%, respectively.

### 2.2 | Ambr$^®$15

Ambr$^®$15 is an automated parallel processing bioreactor that can be employed in capturing data, monitoring, controlling culture parameters in different experiments. The sensors in cooled workstation monitor culture temperature range with individual set point, closed-loop control of pH and DO, independent control of O$_2$, CO$_2$, and N$_2$ for each microbioreactor. There are user defined temperature and stirring set point for each culture station with extended low speed stirring range, from 150 to 2500 rpm. The workstation consists of an Integrated Ambr$^®$ Analysis Module for automated at-line pH calibration and in-process checks and Integrated ViCell XR and Cedex HiRes cell counters. Ambr$^®$15 Liquid Handler Automated liquid handling robotics (LHR) manage all liquid transfer steps during the culture process: media, feed, and reagents are dispensed using 1 and 5 ml sterile pipette tips—samples are taken from the microbioreactors using 1 ml sterile pipette tips—larger volumes of microbioreactor culture are removed in a single step using the Rapid Vessel Drain. Ambr$^®$15 microbioreactor vessel Mimics the characteristics of lab scale bioreactors to enable optimal cell growth, productivity and product quality. Each vessel with sparge tube for gassing into impeller mixing zone, or without for headspace gassing has the capacity of 10–15 ml working volumes.

### 2.3 | Culture analysis

#### 2.3.1 | Cell count and viability

Online cell counting and viability was measured using a Vi-Cell XR (Beckman Coulter, USA) set to the following parameters: minimum diameter (m) = 6, max diameter (m) = 20, cell brightness (%) = 85, cell sharpness = 100%, viable cell spot brightness (%) = 65, viable spot area (%) = 10, minimum circularity = 0.8. The selected parameters for T-cell counts were based on the previous setup for T cell count and literature. A coefficient of variation of 4% was calculated for counts from parallel bioreactor technical replicates. Visual checks (50 images per each count) were conducted to validate the T-cell count identification of the samples. The cell count for two replicates of each sample was carried out every 3 h and initiated at inoculation point in Ambr$^®$15 bioreactor.

#### 2.3.2 | Flow cytometry of T-cells subpopulation markers

Cells from each vessel were sampled ($1 \times 10^5$/tube) into flow buffer containing: phosphate-buffered saline (PBS) and 1% bovine Serum albumin (BSA) and centrifuged at 300$g$ for 10 min following removal of dynabeads. Cell pellets were resuspended and mixed with the appropriate volume of antibodies to a final volume of 100 μl in flow buffer. The Antibody Panel consisted of 1.1 μl of CD8-VioGreen 500 nm human, CD4-PerCP-Vio700nm human Clone REA623, CD45RO-APC-Vio770 nm human Clone REA611, CD45RA-PE-Vio770 human Clone REA562 and CD197 (CCR7)-VioBlue 450 human clone REA546 per $1 \times 10^5$ cell 20 μl$^{-1}$ cell suspension samples (Miltenyi Biotec, DE). Cells were incubated for 10 min at 4°C, washed once with flow buffer and analyzed using a BD FACSCantoTM II flow

cytometer (BD Biosciences, USA) and gated against specific isotype and fluorescence-minus-one controls.

### 2.3.3 | Specific consumption/production rate of Metabolites

Duplicate metabolites samples were collected daily from each vessel (500 μl) and were centrifuged at 300 g for 10 min. The supernatant containing spent media was collected and stored at $-20°C$ prior to analysis. Spent media was analyzed for glucose and lactate using the Cedex Bio-HT (Roche, DE) to calculate the specific metabolite rate mmol cell$^{-1}$ days$^{-1}$.

### 2.4 | Modeling and model evaluation for manufacturing

#### 2.4.1 | Unstructured ODE model

Hypotheses for alternative mechanisms of cell growth and growth inhibition were proposed (as described in the results) and expressed mathematically using a tailored Ordinary Differential Equation (ODE) modeling framework previously described.[18,19] T-cells in the Ambr®15 bioreactor were subject to varying media exchange and initial density culture regimes and cell counts recorded. Candidate models were fitted to minimize least squares deviation. The model was iterated to both validate original parameters and include additional explanatory elements such as the nutrient glucose.

In brief, an ODE paradigm was used to model the evolution of system components over time. Media or cell density change operations were modeled as step changes in, with forward Euler used to obtain model variable evolution between these time-points. Optimization was performed via an exhaustive search of parameter space (i.e., a brute force screen of all combinations of parameter values). An acceptable model fit was considered to show no gross systematic deviations in residuals across the model experimental space.

#### 2.4.2 | BioSolve process

The economics of optimal process options for media exchange regimes and initial culture densities were modeled using BioSolve Process (Biopharm Services, UK) commercial software. BioSolve is a Microsoft® Excel-based software used in the pharmaceutical industry for modeling monoclonal antibodies, vaccines, cell and gene therapies, and products derived from mammalian and microbial production processes.[24,25] This software has an extensive database with default costs, equipment, consumable, and material details, which are updated yearly. The BioSolve Process version 8.0 was used for this evaluation.

The cost analysis presented in this work focused on the cost of goods (CoGs) per million cells generated, and materials categories which included: culture media, dynabeads addition, the starting PBMC

material, and in-process QC tests. The PBMC cost was obtained from Biosolve model and assumed to be 201.38 USD/vial. The process used in Biosolve for the generation of PBMC has been previously described.[26,19] The entire experimental set-up, protocol and results for the T-cell process described in Step 1 of the Materials and Methods section was simulated in BioSolve. This was also the case for the QC tests performed, namely viable cell count and identity by flow cytometry analysis, accounting for 1388.60 USD/batch. The small-scale model based on the Ambr®15 bioreactor system (Sartorius Stedim) used for the experiments shown in this article were scaled-up to a standard 2 L single-use stirred tank reactor cell culture system to quantify the cost impact of optimized process options on a target 2 L scale for autologous T-cell therapy manufacture.

## 3 | RESULTS AND DISCUSSION

Our initial objective was to develop a model that described the T-cell number in the bioprocess over time (yield) in terms of change in the culture environment by the cells. The aim was to determine the quality impact on T-cells of exceeding the point at which growth could be maintained to mirror a manufacturing scenario where medium exchange was delayed or poorly optimized. Modeling the system in terms of unstructured parameters describing cell generated inhibition, rather than in terms of specific nutrients and metabolites, could represent a common scenario early in the process development path. Therefore, this modeling approach is based on growth data that are available in the absence of significant analytical data on the process environment (Figure 1).

### 3.1 | Constructing a simple feed model for T-cell growth and inhibition

A growth rate, a constant specific production rate of an inhibitory factor (arbitrarily set at 1 inhibitory unit produced per $1 \times 10^6$ cell h$^{-1}$), an inhibition of growth rate by generated inhibitory factor units (defined by a threshold and sensitivity parameter), and a cell decay promoted by the same mechanism, were modeled as previously described. Model parameters were optimized by simultaneous fitting of experimental datasets obtained from T-cells cultured in the Ambr®15 system under diverse operational scenarios including two start culture densities: high-cell density: $1.1 \times 10^6$ cell ml$^{-1}$ and low-cell density: $0.6 \times 10^6$ cell ml$^{-1}$ and different medium dilution timings: at 24 or 37 h post inoculation that was described as model 1.

Results from Figure 2 and Table 1 indicated a reasonable fit (assessed visually by good trend following with no large systematic deviation in residuals with time or across experimental conditions; growth rate: 0.012 cell h) with a simultaneous and common parameter optimization across all experimental conditions. The model 1 and experimental data suggested that culture growth rate could be approximated as a function of cell time in the system with a high degree of confidence and its consistent with a cell driven exhaustion of the medium. Cells proliferated exponentially in both medium dilution timing scenarios at 24 and 37 h before
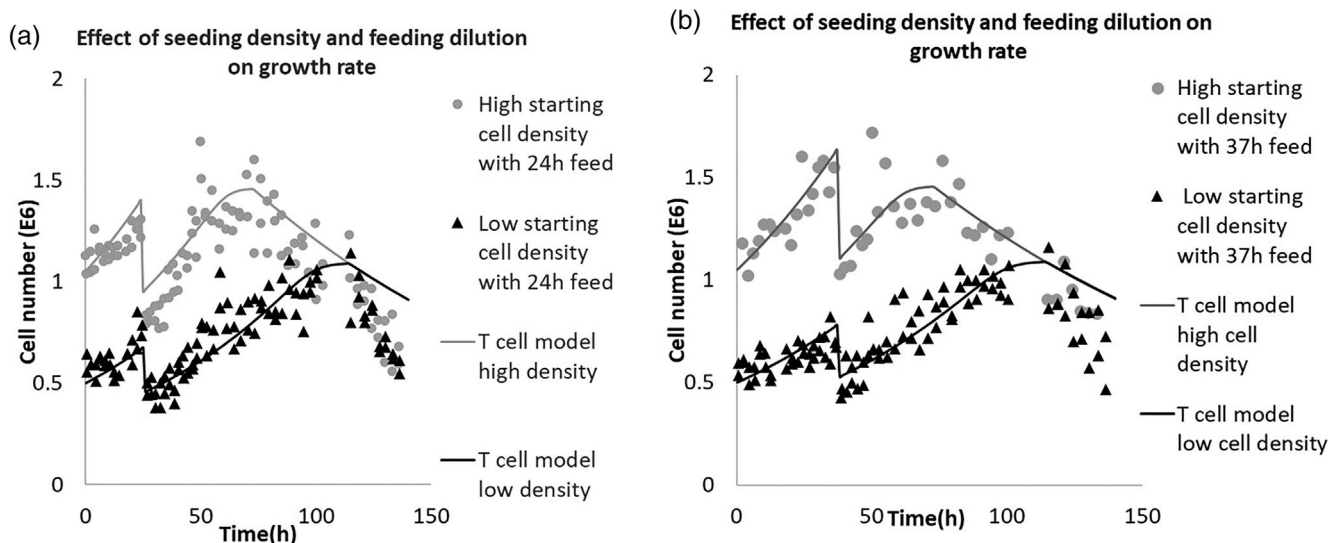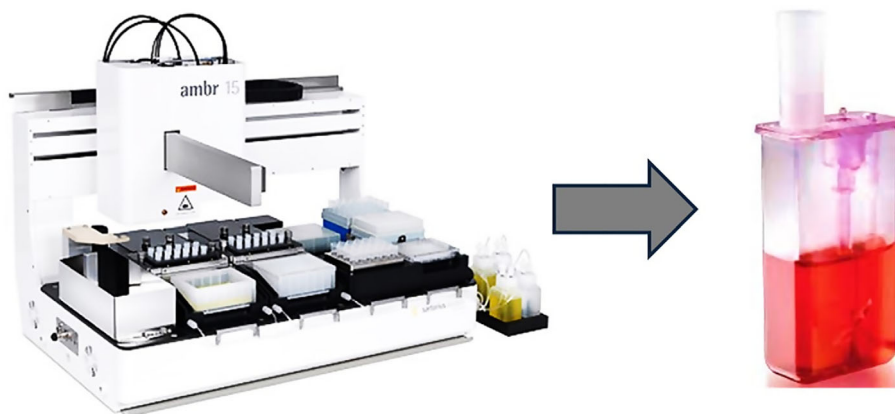
**FIGURE 2** Growth of T-cells reseeded into fresh culture medium in the Ambr®15 bioreactor at two different initial culture densities (high-cell density: $1.1 \times 10^6$ cell ml$^{-1}$ and low-cell density: $0.6 \times 10^6$ cell ml$^{-1}$) and with different timing of a dilution feed. (a) 0.33 proportional volume dilution at 24 h post inoculation, (b) 0.33 proportional volume dilution at 37 h post inoculation. Lines represent a model 1 fit of cell growth, growth inhibition, and cell death based on cell mediated medium exhaustion

entering the inhibition phase at around 73 and 120 h post inoculation in high cell density and low cell density conditions. Beyond the inhibition point, T-cells growth declined significantly as a sign of system exhaustion with the number of cells reached to below the initial seeding density ($0.7 \times 10^6$ cell ml$^{-1}$). However, as expected starting seeding density had a dominant impact on time to system exhaustion with T-cells in the high cell density scenario entering the inhibition phase much earlier than cells in low seeding density condition in both feeding dilution strategies. Overall, model 1 suggests an ability to predict system exhaustion as a function of operational parameters starting cell density and dilution time.

## 3.2 | Development of a glucose dependent Monod model for T-cell growth and inhibition

Given the initial model suggested cell activity driven was by growth inhibition, it was probable that this was due to depletion of a key

nutrient or accumulation of a toxic metabolites (Figure 2a,b). Without overcoming this inhibition, the model implies that bulk batch medium exchange will limit T-cell volume productivity to approximately $1 \times 10^6$ cells produced per ml of volume exchanged. Preliminary analysis of medium sampled during model 1 development indicated rapid depletion of glucose; thus, it was hypothesized that glucose availability could directly be modeled to predict cell growth. A new glucose dependent model was defined describing the system as T-cells including: a growth rate, a constant specific consumption rate of glucose, a promotion of T-cell growth rate by glucose (defined by Monod kinetics), a promotion of glucose consumption rate by T-cells (defined by Monod kinetics) and a cell decay rate inhibited by glucose (defined by a threshold and sensitivity parameter as previously described). Once again, glucose dependent model parameters were optimized using fitting of simultaneous experimental datasets obtained from T-cells cultured in the Ambr®15 system which represent different start culture densities (high-cell density: $0.8 \times 10^6$ cell ml$^{-1}$ and low-cell

**TABLE 1** Range and resolution of optimized input parameter values for model 1

| Parameter | Value | Unit |
|---|---|---|
| Growth rate (GR) | 0.012 | $h^{-1}$ |
| Death rate | 0.007 | $h^{-1}$ |
| Creation of inhibition (arbitrary) | 1 | Inhibition units created. Million cell $h^{-1}$ |
| Threshold of growth inhibition | 63 | Inhibition units |
| Sensitivity of growth inhibition | 0.4 | Unitless (modulator of inhibition) |
| Threshold of death promotion | 80 | Inhibition units |
| Sensitivity of death promotion | 4000 | Unitless (modulator of promotion) |

*Note*: The values for variety of parameters including growth rate, threshold and sensitivity for growth inhibition, and promotion of cell death were explored to define the optimized values for model variables.[17,18] Best fit: GR = 0.012, GR thresh = 63, GR taut = 0.4, Death rate = 0.007, Death thresh = 80, Death taut = 4000.

**TABLE 2** Optimized parameter values for model 2 (Monod kinetics) that implies glucose can be fed slower than 0.05 and growth will continue[17]

| Parameter | Value | Unit |
|---|---|---|
| GR | 0.01 | $h^{-1}$ |
| Glc Sp rate | 0.05 | mg million cell $h^{-1}$ |
| Monod Glc_GR | 0.005 | mg $ml^{-1}$ |
| Decay Glc threshold | 0.05 | mg $ml^{-1}$ |
| Monod Glc_GLc use | 0.2 | mg $ml^{-1}$ |
| Decay Glc taut | 30 | |
| Cell decay | 0.007 | $h^{-1}$ |

Abbreviations: Glc, glucose; Glc Sp rate, glucose specific consumption rate; GR, specific growth rate; Monod Glc_GR, Monod constant determining specific growth rate as a function of Glc concentration (i.e., concentration of glucose at which specific growth rate is half maximal [half-effect]); Monod Glc_GLc use, Monod constant determining specific glucose consumption as a function of glucose concentration (i.e., concentration of glucose at which specific glucose consumption rate is half maximal).

density: $0.375 \times 10^6$ cell $ml^{-1}$) and different medium dilution timings (24 or 37 h) to support robust parameter optimization across different operational scenarios. Optimized parameter values and optimized model fit to data are shown in Table 2 and Figure 3. The glucose dependent model predicted cell growth based on variation in initial cell density and feeding rates and indicated that cell growth linked to metabolites specific consumption/production rate.

The parameter optimization for the Monod kinetics indicated that the concentration of glucose at which the specific rate of glucose use rate is half the maximal (half-effect...) was significantly higher than the glucose concentration that was inhibitory for growth or caused cell death (half-effect, threshold) (Figure 3a–e). These findings suggested

that delivery of glucose at a feed rate significantly under the maximum specific consumption parameter value of 0.05 mg $1 \times 10^6$ cell $h^{-1}$ should adequately sustain growth as consumption rate of glucose will reduce before detrimental concentrations are reached.

## 3.3 | Validation of glucose supply model

To validate the effect of glucose concentration on T-cell growth, a further culture was conducted in which glucose was provided using different feed strategies including: a 1% $h^{-1}$ dilution of standard glucose medium (glucose concentration: 2.06 mg $ml^{-1}$), a 1.13% $h^{-1}$ dilution with high-glucose medium (glucose concentration: 4.11 mg $ml^{-1}$) and a 0.57% $h^{-1}$ dilution with extra high-glucose medium (glucose concentration: 8.22 mg $ml^{-1}$) (Figure 4a–c). In the latter 2 conditions the total glucose delivery remained the same and targeted to initially deliver the 0.05 mg $1 \times 10^6$ cell $h^{-1}$ which was consumed by the cells in the previous experiment and in the presence of excess glucose. The first scenario of standard medium at 1% $h^{-1}$ would deliver 0.02 mg $ml^{-1}$ $h^{-1}$ glucose to the cells which was approximately 50% under the calculated T-cells glucose consumption rate in the previous experiment. The design of experimental conditions was based on the ODE model calculations that the initial seeding density of T-cell culture at $0.8 \times 10^6$ cell $ml^{-1}$ would require 0.04 mg $ml^{-1}$ $h^{-1}$ glucose supplementation from the start with assumption of 0.05 mg $1 \times 10^6$ cell $h^{-1}$ for glucose consumption rate.

The data were tested against the same model and optimized parameter values as previously defined. The growth rate required adjusting due to faster proliferation (0.17 $h^{-1}$) but all other model parameters with respect to metabolic behavior remained the same. Data fit to the model was reasonable for the low-glucose delivery, suggesting an adequate parameter optimization from the initial data set and confirming that an 'undersupply' of glucose sustained the continual growth rate over the full culture period—even though by the end of the culture period delivery rate was approximately 25% of the suggested feed based on optimized specific consumption rate parameter (Figure 2a). Further, the cultures with glucose delivered closer to the measured consumption rate both became growth inhibited early, seen as a lack of fit of cell numbers and glucose relative to the model predictions. Inhibition at a similar time point despite the different bulk dilutions suggested that this is related to the glucose supply (which was matched) rather than any other factor (Table 3).

## 3.4 | Development of an optimized glucose supply model of T-cell growth and inhibition

To confirm the robustness of the model to multiple inputs, and further establish the sensitivity of the system to glucose supply, a further experiment was conducted in which 1% $h^{-1}$ dilution feeds with glucose at 2.056, 2.467, and 2.878 mg $ml^{-1}$ were supplied to each vessel. Once again, the lower rate of glucose provision sustained the culture in line with the model predictions, with the higher glucose provision causing earlier growth reduction (Figure 5a–c).
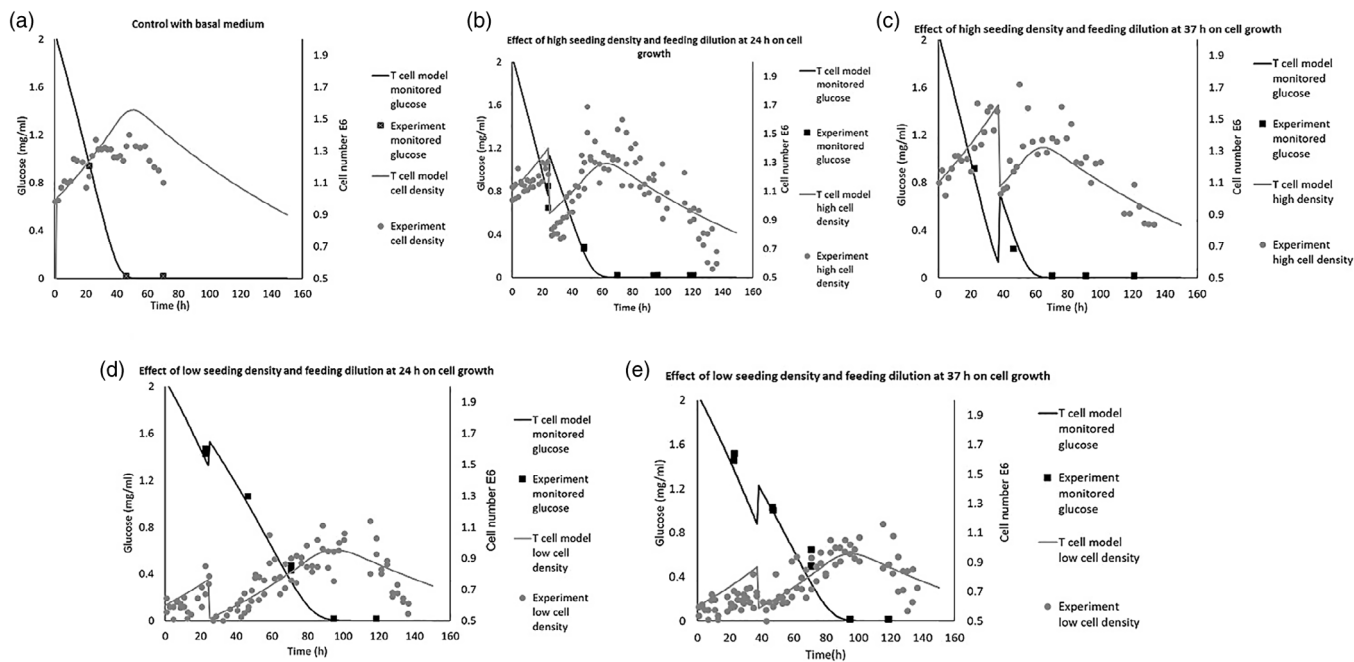
**FIGURE 3** Growth curves of T-cells and glucose depletion model 2 (glucose dependant, Monod kinetic model) from different initial culture densities (high-cell density: $0.8 \times 10^6$ cells ml$^{-1}$ and low-cell density: $0.275 \times 10^6$ cells ml$^{-1}$) and with different timing of a dilution feed with no added glucose. Lines represent a model fit of cell growth and inhibition based on glucose depletion. (a) No feed and no cell dilution, (b) 24 h feed 0.33 dilution, high density, (c) 37 h feed 0.33 dilution high density, (d) 24 h 0.33 dilution low density, (e) 37 h feed 0.33 dilution low density
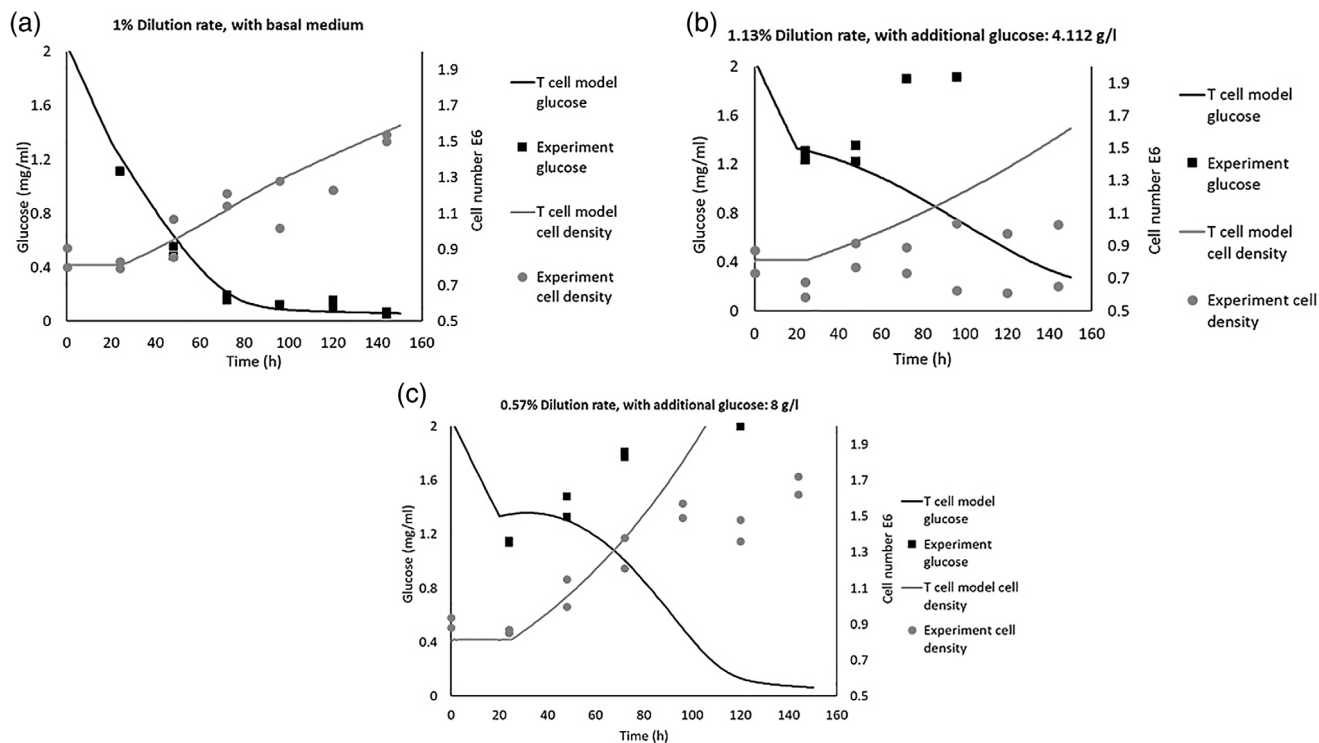


**FIGURE 4** Growth curves of T-cells and glucose depletion in model 3, (glucose supply model) with different feeding dilution rates and glucose concentration in the bulk medium. (a) 1% dilution rate with 2.056 mg ml$^{-1}$ glucose, (b) 1.13% dilution rate with 4.112 mg ml$^{-1}$ glucose, (c) 0.57% dilution rate with 8 mg ml$^{-1}$ glucose. Showing that glucose supplied at a lower rate than the maximal consumption rate established in the glucose feed model sustains growth longest indicating a substantially lower glucose demand than that consumed at higher glucose concentrations

The results of optimized glucose model indicated that glucose reached a steady-state level at approximately 100 h post inoculation in all conditions, but the level at which the glucose stabilized varied and depended on the rate of glucose delivery. This was evident by measurement of higher glucose concentration in the bulk medium in

conditions with feed at 2.4 and 2.8 mg ml$^{-1}$ at steady state level. These findings qualitatively validated the experimental results of the optimized glucose supply strategies which indicated the highest glucose concentration at the steady state level in 2.8 mg ml$^{-1}$ feeding scenario (0.5 mg ml$^{-1}$) in comparison to the measured glucose in 1% h$^{-1}$ dilution feed with no added glucose (0.2 mg ml$^{-1}$).

The optimized glucose supply model showed that the increased glucose concentration in the feeds sustained the growth beyond the lower glucose provision in the native medium. However, despite maintaining steady state glucose at different levels both conditions became growth inhibited around 140 h suggesting a further inhibitory factor beyond glucose availability. Beyond this point, T-cells growth continued to decline considerably due to the system exhaustion and cells number did not recover from day 5 post inoculation (Table 4).

**TABLE 3** Optimized parameter values for model 3 that glucose is detrimental at 1.13% feeding rate and inhibits cell growth

| Parameter | Value | Unit |
| --- | --- | --- |
| GR | 0.017 | h$^{-1}$ |
| Glc Sp rate | 0.08 | mg million cell h$^{-1}$ |
| Monod Glc_GR | 0.005 | mg ml$^{-1}$ |
| Decay Glc thresh | 0.05 | mg ml$^{-1}$ |
| Monod Glc_GLc use | 0.2 | mg ml$^{-1}$ |
| Decay Glc taut | 30 | |
| Cell Decay | 0.007 | h$^{-1}$ |

*Note*: 1% feeding rate with no glucose addition shows no growth inhibition.[17]
Abbreviations: Glc, glucose; Glc Sp rate, glucose specific consumption rate; GR, specific growth rate; Monod Glc_GR, Monod constant determining specific growth rate as a function of Glc concentration (i.e., concentration of glucose at which specific growth rate is half maximal [half-effect]); Monod Glc_GLc use, Monod constant determining specific glucose consumption as a function of glucose concentration (i.e., concentration of glucose at which specific glucose consumption rate is half maximal).

## 3.5 | The impact of T-cell's culture parameters on phenotypic commitment

### 3.5.1 | Monod Kinetics model

In the Monod Kinetics model, Comparison of phenotypic data between static culture and Ambr®15 system's different feeding frequency and seeding density conditions showed sensitivity of SCM/TCM, TEM and effector populations in both CD4$^+$ and CD8$^+$ subsets (Figure 6a,b). However, CD8$^+$ subpopulations changed more significantly over time
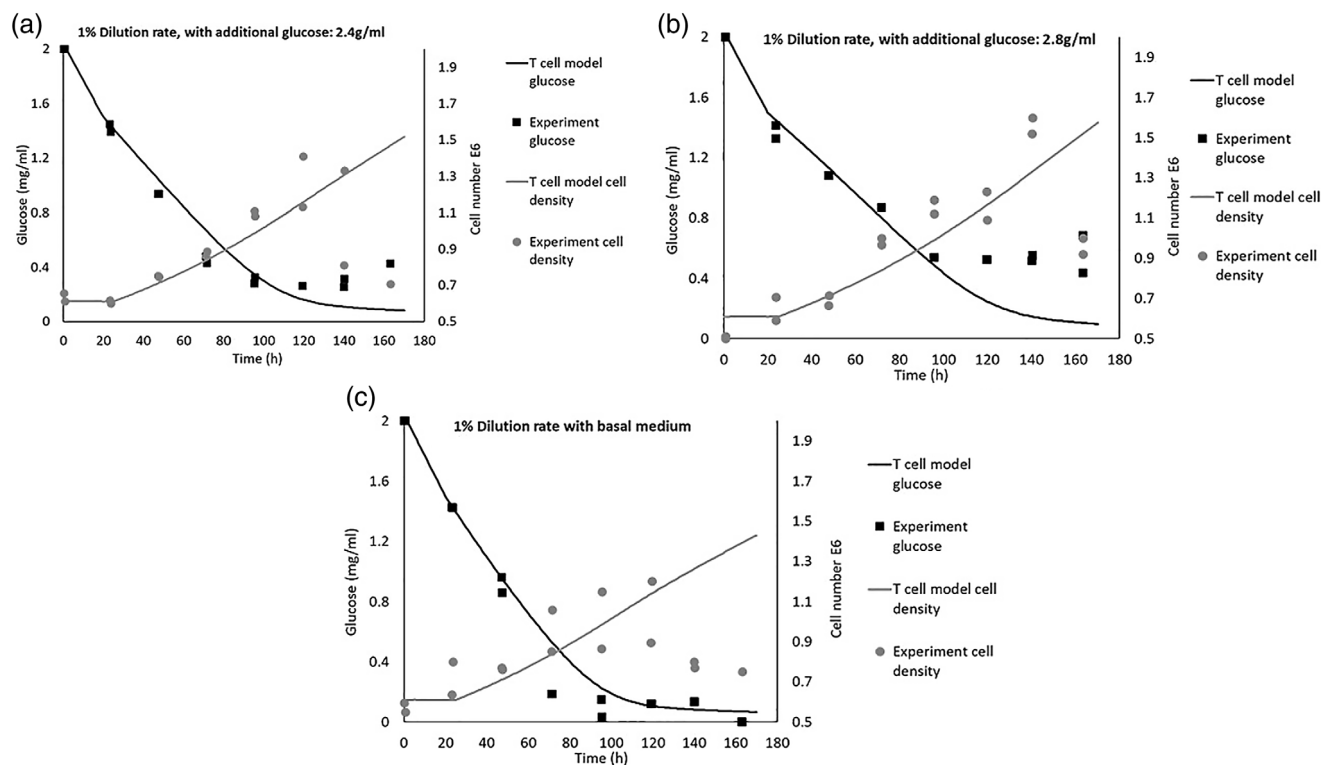


**FIGURE 5** Growth curves of T-cells and glucose depletion in model 4, (optimized glucose supply model) with different feeding dilution rates and glucose concentration in the bulk medium. (a) 1% dilution rate with 2.4 mg ml$^{-1}$, (b) 1% dilution rate 2.84 mg ml$^{-1}$ glucose, (c) 1% dilution rate with 2 mg ml$^{-1}$ glucose (no added glucose). Validation that glucose is not restrictive; give glucose at normal 20% and 40% above base feed

**TABLE 4** Optimized parameter values for model 4 (optimized glucose supply model) that shows growth rate is higher as is glucose consumption

| Parameter | Value | Unit |
| --- | --- | --- |
| GR | 0.015 | h$^{-1}$ |
| Glc Sp rate | 0.05 | mg million cell h$^{-1}$ |
| Monod Glc_GR | 0.005 | mg ml$^{-1}$ |
| Decay Glc thresh | 0.05 | mg ml$^{-1}$ |
| Monod Glc_GLc use | 0.2 | mg ml$^{-1}$ |
| Decay Glc taut | 30 | |
| Cell Decay | 0.007 | h$^{-1}$ |

*Note*: This validation reveals that glucose was not restrictive and approximately the same restriction points in all three conditions imply total dilution rather than glucose concentration being the issue.[17] Abbreviations: Glc, glucose; Glc Sp rate, glucose specific consumption rate; GR, specific growth rate; Monod Glc_GR, Monod constant determining specific growth rate as a function of Glc concentration (i.e., concentration of glucose at which specific growth rate is half maximal [half-effect]); Monod Glc_GLc use, Monod constant determining specific glucose consumption as a function of glucose concentration (i.e., concentration of glucose at which specific glucose consumption rate is half maximal).

that was evident by a sharp decline of SCM/TCM population (*p* value: 0.016) followed by an increase in both effectors, Naive and TEM populations between day 2 and day 5 (*p* value: 0.001 and 0.016, respectively). In addition, the results of statistical analysis suggested that starting seeding density had a dominant influence on effector and SCM/TCM populations and CD4$^+$/CD8$^+$ ratio (*p* value: 0.002 and 0.003) (Table S1). Other subpopulations including CD4$^+$ TEM, CD8$^+$ SCM/TCM were also sensitive to variation in starting cell density but change in dilution frequency had minimum effect in shifting the T-cell subpopulations as only CD8$^+$ SCM/TCM expression level changed significantly over time (*p* value: 0.041) (Figure 6a,b).

## 3.5.2 | Glucose supply model

Phenotype analysis of the glucose supply model revealed that regardless of the fluctuation in both CD4+ and CD8$^+$ SCM/TCM populations in different dilution feed scenarios, there were no substantial phenotype shift in any of the feed condition (Figure 6c,d). Some subpopulations seemed to be more sensitive to the effect of time in culture including CD4$^+$ subset and CD8$^+$ effector populations that manifested as an increase between day 3 and day 6 post inoculation in all feeding conditions (*p* value: 0.005, 0.001, and 0.001, respectively) (Table S2). This finding was in contrast with percentage of CD4$^+$ SCM/TCM populations that declined in all feeding conditions at the later timepoints (D3–D6) and when T-cells entered the exhaustion phase in the culture. Irrespective of feeding conditions, all CD4$^+$ sub populations increased over time and exhibited the highest growth by day 6 post inoculation (Figure 6c,d).

CD4$^+$/CD8$^+$ ratio was significantly changed over time in all feeding dilution condition (*p* value: 0.049 and 0.001) while no meaningful

phenotypic changes were reported between different feeding dilutions and glucose supply conditions (Figure 6c,d). This was evident as only CD8$^+$ TEM subpopulation showed significant sensitivity to different dilution rate and glucose supply conditions between day 3 and day 6 (*p* value: 0.045) (Table S2).

## 3.5.3 | Optimized glucose supply model

In the optimized glucose supply model, CD8$^+$ subpopulations showed more sensitivity to variation in feeding dilution and additional glucose in T-cell culture at later timepoints in comparison with CD4$^+$ (Table S3). Evidently, only CD8$^+$ SCM/TCM population were significantly influenced by the increase in concentration of glucose in the bulk medium while other factors including dilution rates and time showed to be less effective in influencing T-cells sub-populations. Phenotype analysis at the point of growth inhibition at day 7 showed a strong selective effect on CD8$^+$ cells over CD4$^+$ indicating a relatively high sensitivity of CD8$^+$ to limitation in nutrient supply and culture exhaustion as detailed in Figure 6e,f.

Phenotypically, there was no detected difference in any of the conditions sensitivity to both time and dilution rates between day 3 and day 6 prior to the point of growth inhibition excluding the CD8$^+$ TEM population. This finding suggested that there was no short-term driving effect of cell time accumulation on phenotype in the optimized glucose supply model (Figure 6e,f). CD4$^+$/CD8$^+$ ratio varied significantly at the later time points in culture prior to and after cells entering the inhibitory in all feeding scenarios while, additional glucose proved to have a less dominant effect in variation of CD4$^+$/CD8$^+$ ratio. Unlike most of CD4$^+$ subpopulations that showed no statistically significant changes over the time, dilution or glucose supply conditions, CD8$^+$ SCM/TCM and TTEM populations manifested substantial variation between growth and inhibition phases in all scenarios (*p* value: 0.020 and 0.010, respectively) (Table S3).

Comparison of phenotypic changes between Monod Kinetics model, Glucose supply and the optimized glucose supply model revealed that apart from CD8$^+$ effector population sensitivity over time, there were no commonalities in the influence of feed, or glucose supply on different T-cell sub populations. In contrast, time in culture proved to be the main factor that influences CD4$^+$/CD8$^+$ ratio in both glucose and optimized glucose models. Unlike CD4 populations that remained stable between growth and inhibition phase, CD8$^+$ populations showed more significant variation over time in all three feed models.

Phonotypic data analysis of Monod Kinetics and optimized glucose supply models suggested that CD4$^+$ effector populations were markedly affected by both change in feeding dilution and initial seeding density in culture (*p* value: 0.023 and 0.005, respectively), whereas CD8$^+$ naïve populations were mostly sensitive to the time in culture and transition from growth phase to exhaustion in both models (*p* value: 0.001 and 0.024).

Despite some commonalities between the effect of different feeding and glucose supply conditions on selection of CD4$^+$ and
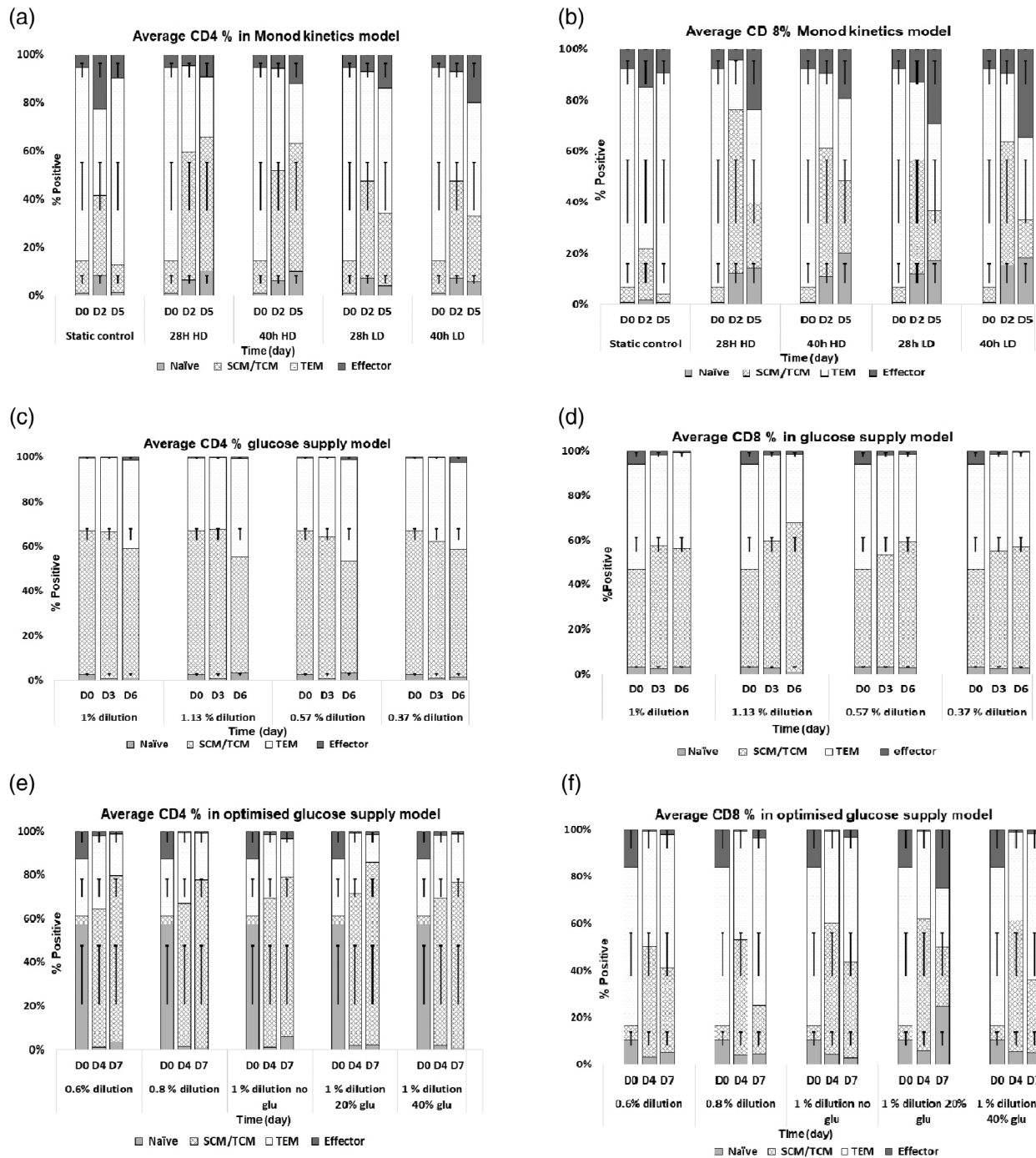
**FIGURE 6** Results of phenotype variation in CD4^{+} and CD8^{+} T-cells cultured under different dilution rates and glucose concentration in the bulk medium for (a and b) Monod kinetics model, (c and d) glucose supply, and (e and f) optimized glucose supply models. Adjusting the feeding rates did not appear to have any effect on diverging the T-cells' subpopulation growth. Variation in T-cells' starting subpopulations seems to dictate the outcome of process regardless of provision of glucose supply and feeding strategies

CD8^{+} sub populations, variation in the initial phenotypic data from the same donor seemed to have the main influence on the outcome of the process. Differences in phenotypic pool of T-cells after the manual expansion and prior to inoculation massively dictated the expression level of subpopulations at later time point of culture and beyond other parameters including dilution rates, starting seeding density and additional glucose supply.

## 3.6 | Scaling up T-cell process: Applications of a cost model in manufacturing settings

The ODE model data were used to inform volumes and densities as input to a Biosolve process model operating at a theoretical 2 L scale (Figure 7). The volume productivity of a cell culture medium (cells that can be produced per ml of volume exhausted) defines the
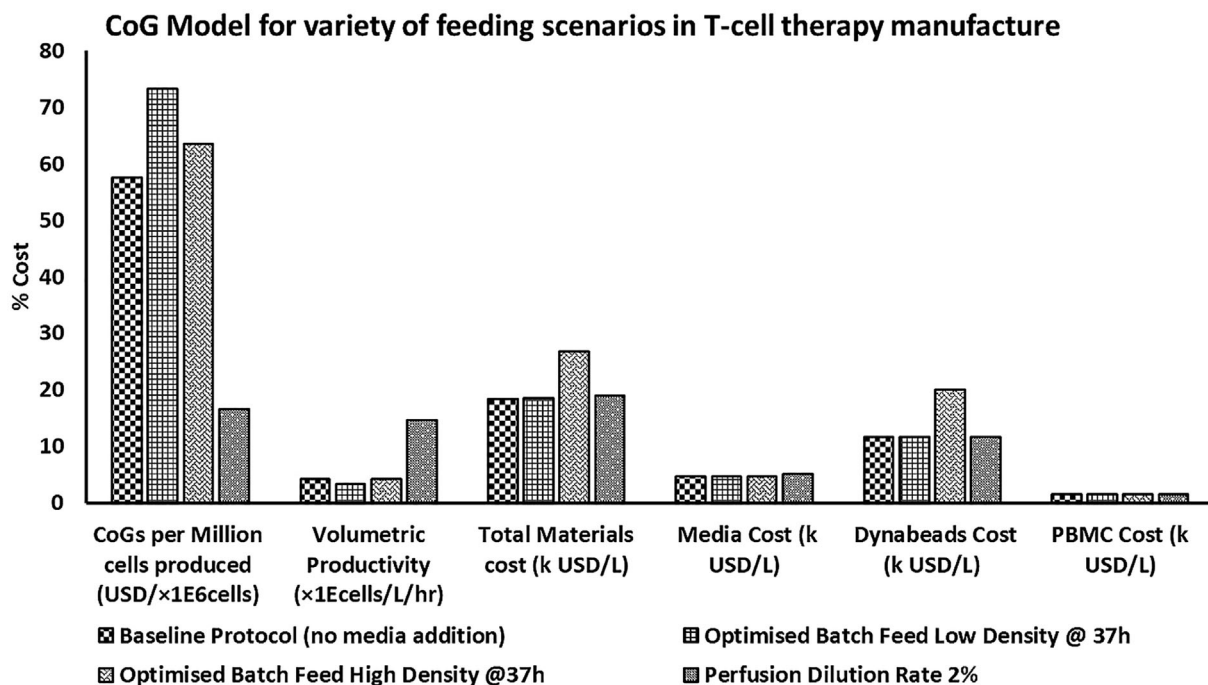
## CoG Model for variety of feeding scenarios in T-cell therapy manufacture



**FIGURE 7** The results of CoGs, volumetric productivity and costs of materials derived from BioSolve process model (Biopharm Services, UK) for optimal T-cell processes at 2 L bioreactor scale. Perfusion process was the most cost-effective process with lowest CoGs per million cells and highest volumetric productivity. Optimal T-cell processes: Baseline protocol with no media addition and low-cell density of $0.5 \times 10^6$ cells ml$^{-1}$. Low-cell density: $0.5 \times 10^6$ cells ml$^{-1}$, high-cell density: $1.0 \times 10^6$ cells ml$^{-1}$, perfusion culture with dilution rate of 2% was assumed to be consisted of low-cell density: $0.5 \times 10^6$ cells ml$^{-1}$

combination of bioreactor volume and volume exchange rate required to deliver a given yield of product (Figure 7). Without a change in volume productivity of medium, then a reduction in bioreactor volume must be matched with a proportional increase in fluid exchange. The initial model of batch exchange, both non-specific and glucose dependent, indicated a volume productivity of approximately $1.5 \times 10^6$ cell ml$^{-1}$. The low-glucose feed has a significant impact on volume productivity. The 1% h$^{-1}$ feed rate with 2.056 g L$^{-1}$ glucose supported $3 \times 10^6$ cell ml$^{-1}$, increasing the number of cells that can be yielded from a given bioreactor scale for a given rate of medium exchange (Figure 7).

The results of the BioSolve process model indicated that the materials cost category was the biggest cost driver of T-cell process ranging between 23% and 30% after fixed Labor costs (48%–53%), in line with previous published work.[26,19] Scaling up to 2 L scale reduced the resulting CoGs, improved productivity and involved relatively less materials consumption, as it took advantage of economies of scale (results not shown). Perfusion process was found to be the most cost-effective process with highest volumetric productivity and the lowest CoGs per million cells produced (Figure 8a). Even though perfusion had the highest relative consumption of media, the higher final cell densities achieved at the end of the perfusion process drove productivities up and resulted in lower costs (16.5 USD/million cells). The Optimized Fed-batch low-density process with single addition at 37 h achieved the highest CoGs and lowest productivity. As mentioned previously, this was driven by the low final cell densities achieved by

this process. This optimized process option had the highest materials cost derived from higher requirements of dynabeads—a factor of higher starting cell densities.

The results of sensitivity analysis revealed that final cell density had the highest impact upon final CoGs per million cells for all optimized scenarios that were evaluated by the BioSolve model. It also indicated that the dynabeads cost per Kg also had a very significant impact on the final CoGs. These changes impacted the optimal scenarios with a higher starting cell density more significantly and similarly to the effect of changes in dynabeads addition ratio in T-cell culture (Figure 8).

## 3.7 | Applications of a simple unstructured ODE model on T-cell growth and phenotypic commitment

Application of a simple unstructured model of T-cell growth in a stirred tank system was explored in this article. The first iteration of the model can provide an operator with a framework for operation with respect to timings and volume of medium delivery to maintain an uninhibited growth. The Second iteration indicates how glucose delivery can be controlled to sustain cell growth. Furthermore, through showing the (predominantly CD4$^+$) population selective effects of exceeding the supported growth period, the model informs risk assessment of process operation on product quality. It was proposed that model is developed hierarchically and systematically (Table S4).
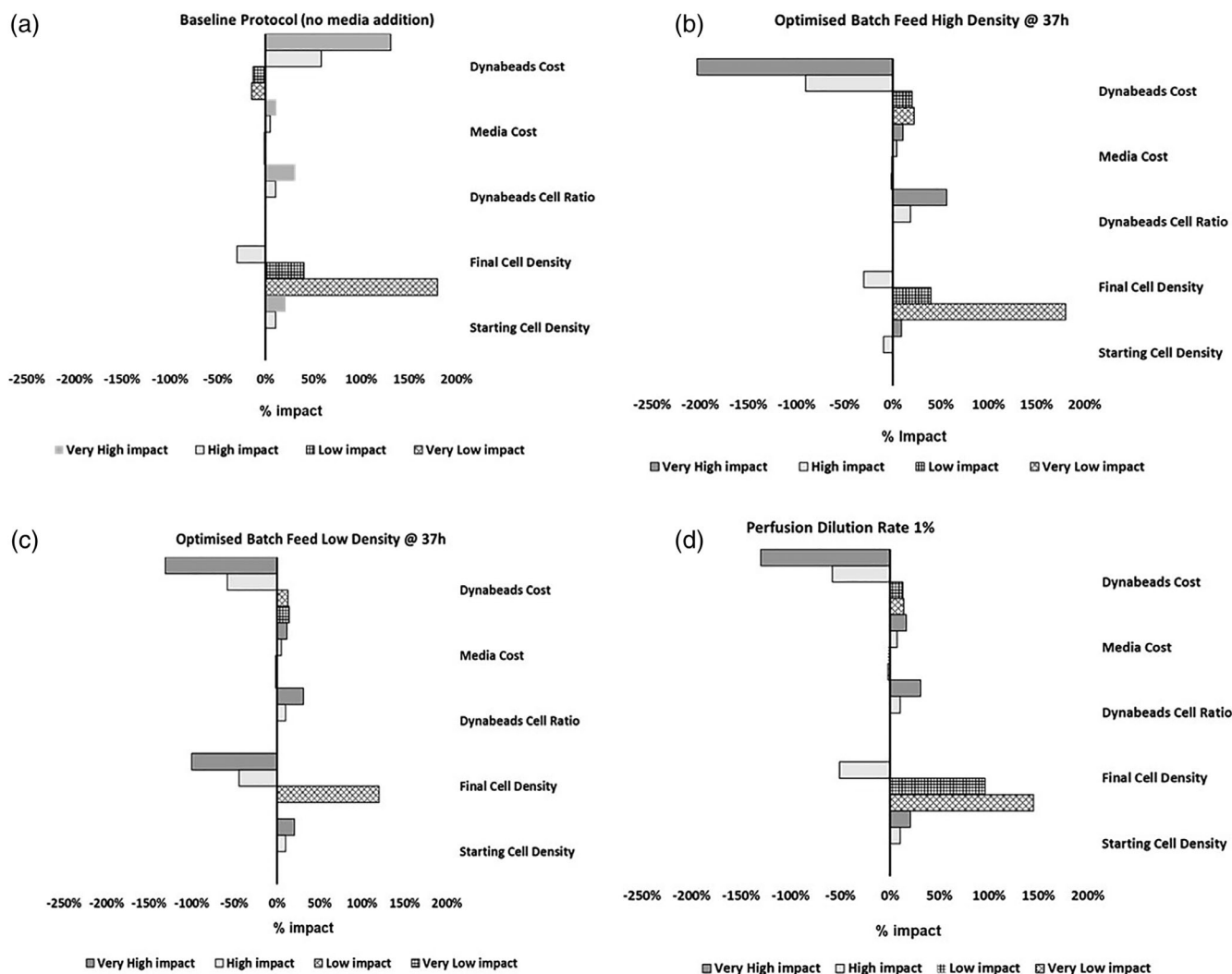
**FIGURE 8** The results of sensitivity analysis derived from BioSolve process model (Biopharm Services, UK) for optimal T-cell processes at 2 L bioreactor scale. Initial cell density and dynabeads were found to have the biggest impact upon resulting CoGs per million cells. (a) Baseline protocol with no media addition and low-cell density of $0.5 \times 10^6$ cells ml$^{-1}$. The cell density of the optimized batch feeds at 37 h was assumed as (b) $0.5 \times 10^6$ cells ml$^{-1}$ and (c) $1.0 \times 10^6$ cells ml$^{-1}$ for low- and high-cell density, respectively. (d) Perfusion culture with dilution rate of 2% consisted of low-cell density: $0.5 \times 10^6$ cells ml$^{-1}$. Variables used for sensitivity analysis include: starting cell density (up to $1.5 \times 10^6$ cells ml$^{-1}$), final cell density ($5.0 \times 10^5$–$1.0 \times 10^7$ cells ml$^{-1}$), dynabeads cell ratio (up to 1:4), and cost of media per liter and dynabeads per Kg (100 times decrease up to 10 times increase in cost). High, very high, low, and very low in graphs refer to the qualitative significance of variables impact on CoGs

Initially, the rate at which culture medium would need to be exchanged to maintain cell growth was determined (simple feed model). The finding from the feed model indicated gross system behavior without identification of individual components.

Variation in starting material and proportion of subpopulations resulted in different outcome at end points regardless of effect of different experimental condition including: dilution rate and frequency and addition of glucose in the bulk media. Analysis of Flow cytometry data demonstrated variation in percentage of CD4$^+$, CD8$^+$, and T-cell subpopulations at D0. These batch-to-batch deviations caused diverse outcome for T-cell sup-population proportion for model 1 and model 2 experiments with identical starting cell density and feeding conditions. Phenotype analysis of experimental data demonstrated that cell

density seemed to have a leading effect in supporting the clinically relevant T-cell subpopulations when compared with the feeding time. The effect of seeding density was opposite in two subsets of T-cells: CD4$^+$ and CD8$^+$. CD8$^+$ T-cells exhibited higher percentage of TEM, effectors and naive cells in at later timepoints particularly in LD conditions. Higher cell density supports higher percentage of TSCM/TCM populations of T-cells at later time points (D2 and D5) while low-cell density encouraged the growth of more mature T-cells including TEM and effector T-cells. However, time of feeds appeared to have less significant effect on growth of CD4$^+$ sub populations.

The results from different dilution feed with additional glucose supply suggested that provision of glucose in the bulk medium is one of the key factors that supports T-cell growth and proliferation.

Therefore, limitation in glucose supply act as the first inhibitory element in T-cell culture and triggers cell death when T-cells reach the exhaustion phase. However, our data also indicated T-cells can utilize glucose at very low concentrations; this finding is in line with the results of other studies as Thompson et al. demonstrated that even at 0.02 mM glucose, can support T-cell proliferation and viability.[27,28]

The data from the ODE model demonstrated a higher volume productivity in dilution glucose feed scenario in comparison with batch exchange conditions. The dilution per volume unit was reported as 3.36 at 140 h post inoculation. This finding highlighted that 1% dilution feed is more efficient model with higher growth rate and cell hour supported per volume unit. Cells reached inhibition phase in 1% feed glucose model regardless of glucose concentration which underline the role of secondary and tertiary inhibitory factors that prevent cell growth or initiate the cell death in the culture once glucose is optimized. In batch exchange model higher initial cell density reached the limit ($6 \times 10^7$ cells h$^{-1}$ ml$^{-1}$) after 48 h whereas lower seeding density with the same growth rate reached the inhibition at later time points (72 h). This finding suggests that initial cell density is one of crucial elements in determining the extent of T-cell growth and exhaustion phase hence efficiency of the process.

T-cells have a cytoplasmic pool of Glut1 that are transported to the cell surface following activation and is linked closely to a peak in glucose uptake between 48 and 72 h post activation.[29,30] If Glut1 is blocked, the capacity of proliferating naïve T-cells to transform into TSCM is severely compromised. A similar impairment can be caused by inhibition of the mitochondrial pyruvate carrier (MPC) with the small molecule UK5099.[31,29] This indicates that, unlike effector T-cells, TSCM converts glucose into pyruvate and, therefore, does not produce significant amounts of lactate despite high internalization of glucose. As a result, Glut1 blockade could be an effective strategy to generate more selective sub-populations of T-cells such as long-lived TSCM.[3,32] Increased expression of Glut1 and glucose uptake are associated with higher cellular growth and proliferation in thymocytes.[33,34]

Following immune activation, metabolic rates significantly increase in T-cells as a result of proliferative expansion and the production of cytokines.[35,36] This process demands substantial amounts of energy and cellular biosynthesis which leads to an increased demand for nutrients, including glucose, glutamine and amino acids such as serine and arginine, to supply fuel for bioenergetic and biosynthetic pathways.[37,38] Effector T-cells have high rates of glucose and glutamine uptake, which are metabolized by aerobic glycolysis and the tricarboxylic acid cycle.[39,40] Operational costs will be driven down with a smaller unit with less reagents and volume; particularly if allogeneic products take off large batch production costs are driven down. While CD4$^+$ T-cells appear to have selectively increased capacity for mitochondrial respiration of glucose, both CD4$^+$ and CD8$^+$ T-cells can oxidize alternative fuels such as glutamine if required.[41,35] The results of phenotype analysis of CD4$^+$ versus CD8$^+$ population % revealed that the number CD8$^+$ subset increased from ~14% at day 0 to ~22% at day 4 which was followed by a substantial decrease to ~12% at day 7. This indicated that the CD8$^+$ subset might be more sensitive to the effect of inhibitory agents and prior to reaching the

growth inhibition at day 7 as shown in optimized glucose model experiment (Figure 6c,d). These findings are aligned with the results of other T-cell studies which suggest that different T-cell subsets and populations may require a more tailored and specific culture conditions and medium composition in order to support cell growth and to prevent initiation of an premature/undesirable exhaustion.[39,42,43]

Previous cost analysis of cell therapy products using BioSolve saw the same trends seen here, whereby fixed costs were the main cost driver for small-scale operations, irrespective of the type of technology used.[26,19] Secondary drivers were materials costs, highlighting the importance of the optimization of process parameters such as: the quantities of media added, media components, among others. When compared to the author's previous work, the most noticeable impact of the introduction of scalable bioreactor technology in T-cell processing, was the reduction of the costs per million cells produced,[19,20] achieved by the ability to optimize, and improve volumetric productivities. In the context of autologous cell therapies, the resulting cost per batch (or per patient) could be three times higher using these scalable technologies (results not shown).[44] However, the cost benefit of being able to accommodate for the inherent variability of starting cell densities related to the patient cells collected, and the value to maintain tight control over product quality attributes, are yet to be defined upon the cost-effectiveness of the therapeutic. These would be expected to play a significant role in the final process configuration.

## 4 | CONCLUSION

A simple ODE model of cell growth was introduced to specify key parameters for efficient culture operation. It has also demonstrated that this user-friendly model is simple enough to be built and tested with low data and represent the complexity of cell dynamic and biology to a degree that is acceptable for manufacturing applications.

The data from our model indicated that culture growth rate could be approximated as a function of cell time in the system and both starting cell density and timing of feed have a great influence on T-cell system growth and point of growth inhibition.

Furthermore, our model showed that glucose is linked to the growth rate and that a delivery of glucose at a feed rate substantially under the maximal specific consumption parameter value of 0.05 mg $1 \times 10^6$ cell h$^{-1}$ will adequately sustain cell growth in the system.

Data generated by BioSolve model predicted that the optimized glucose supply model can be employed for process optimization in manufacturing settings including 2 L bioreactor scale while providing most cost-effective T-cell process with the lowest CoGs per million cells produced and the highest volumetric productivity.

However, the effect of glucose stochiometric feed and other secondary inhibitory factors in triggering T-cell growth inhibition remains to be explored. For example, presence of other key metabolite factors (lactate, ammonia), amino acids and cytokine concentrations in the bulk media may lead to a delayed growth inhibition and phenotypic commitment in the T-cell system at the later time points. Employing

objective gating strategies including SPADE may shed more lights to the effect of these feeding scenarios and medium compositions on T-cell phenotype data particularly on the clinically relevant subsets and subpopulations.

These results can be further validated by evaluating the impact of stoichiometric feed and optimized cytokines provision on the phenotype of clinical T-cell lines including the virally transduced T-cell and CAR-Ts.

## AUTHOR CONTRIBUTIONS

**Maryam Shariatzadeh:** Conceptualization (lead); data curation (lead); investigation (lead); methodology (lead); software (lead); validation (lead); writing – original draft (lead); writing – review and editing (lead). **Adriana Lopes:** Data curation (supporting); validation (supporting); writing – original draft (supporting). **Katie Glen:** Data curation (supporting); methodology (supporting). **Andrew Sinclair:** Data curation (supporting); investigation (supporting); software (supporting). **Robert Thomas:** Conceptualization (lead); software (lead); supervision (lead); validation (lead).

## PEER REVIEW

The peer review history for this article is available at https://publons.com/publon/10.1002/btpr.3205.

## DATA AVAILABILITY STATEMENT

The data that support the findings of this study are available in [Loughborough University] at [repository.lboro.ac.uk]. These data were derived from the following resources available in the public domain: [repository.lboro.ac.uk].

## ORCID

*Maryam Shariatzadeh* https://orcid.org/0000-0002-0098-6338

## REFERENCES

1. Schulthess D, Gassull D, Makady A, et al. Are CAR-T therapies living up to their hype? A study using real-world data in two cohorts to determine how well they are actually working in practice compared with bone marrow transplants. *BMJ Evid-Based Med*. 2019;26:98-102. https://doi.org/10.1136/bmjebm-2019-111226
2. Seimetz D, Heller K, Richter J. Approval of first CAR-Ts: have we solved all hurdles for ATMPs? *Cell Med*. 2019;11:215517901882278. https://doi.org/10.1177/2155179018822781
3. Ou J, Si Y, Tang Y, et al. Novel biomanufacturing platform for large-scale and high-quality human T cells production. *J Biol Eng*. 2019; 13(1):34. https://doi.org/10.1186/s13036-019-0167-2
4. Rossi J, Paczkowski P, Shen YW, et al. Preinfusion polyfunctional anti-CD19 chimeric antigen receptor T cells are associated with clinical outcomes in NHL. *Blood*. 2018;132(8):804-814. https://doi.org/10.1182/blood-2018-01-828343
5. Di Dedda C, Vignali D, Piemonti L, Monti P. Pharmacological targeting of GLUT1 to control autoreactive T cell responses. *Int J Mol Sci*. 2019; 20(19):4962. https://doi.org/10.3390/ijms20194962
6. Lam C, Meinert E, Yang A, Brindley DA, Cui Z. Decisions in the development lifecycle of cell and gene therapies. *Second Generation Cell and Gene-Based Therapies*. Elsevier; 2020:597-632. https://doi.org/10.1016/b978-0-12-812034-7.00022-4
7. Vander Heiden MG, Plas DR, Rathmell JC, Fox CJ, Harris MH, Thompson CB. Growth factors can influence cell growth and survival through effects on glucose metabolism. *Mol Cell Biol*. 2001;21(17):5899-5912. https://doi.org/10.1128/mcb.21.17.5899-5912.2001
8. Levine BL, Miskin J, Wonnacott K, Keir C. Global manufacturing of CAR T cell therapy. *Mol Ther—Methods Clin Dev*. 2017;4:92-101. https://doi.org/10.1016/j.omtm.2016.12.006
9. Tyagarajan S, Spencer T, Smith J. Optimizing CAR-T cell manufacturing processes during pivotal clinical trials. *Mol Ther—Methods Clin Dev*. 2020;16:136-144. https://doi.org/10.1016/j.omtm.2019.11.018
10. Das R, Roosloot R, van Pel M, et al. Preparing for cell culture scale-out: establishing parity of bioreactor- and flask-expanded mesenchymal stromal cell cultures. *J Transl Med*. 2019;17(1):241. https://doi.org/10.1186/s12967-019-1989-x
11. Somerville RPT, Devillier L, Parkhurst MR, Rosenberg SA, Dudley ME. Clinical scale rapid expansion of lymphocytes for adoptive cell transfer therapy in the WAVE ®bioreactor. *J Transl Med*. 2012;10(1):69. https://doi.org/10.1186/1479-5876-10-69
12. Milone MC, Fish JD, Carpenito C, et al. Chimeric receptors containing CD137 signal transduction domains mediate enhanced survival of T cells and increased antileukemic efficacy in vivo. *Mol Ther*. 2009; 17(8):1453-1464. https://doi.org/10.1038/mt.2009.83
13. Kalos M, Levine BL, Porter DL, et al. T cells with chimeric antigen receptors have potent antitumor effects and can establish memory in patients with advanced leukemia. *Sci Transl Med*. 2011;3(95):95ra73. https://doi.org/10.1126/scitranslmed.3002842
14. Ortolani C, Forti E, Radin E, Cibin R, Cossarizza A. Cytofluorometric identification of two populations of double positive (CD4+,CD8+) T lymphocytes in human peripheral blood. *Biochem Biophys Res Commun*. 1993;191(2):601-609. https://doi.org/10.1006/bbrc.1993.1260
15. Hartigan-O'Connor DJ, Poon C, Sinclair E, McCune JM. Human CD4 + regulatory T cells express lower levels of the IL-7 receptor alpha chain (CD127), allowing consistent identification and sorting of live cells. *J Immunol Methods*. 2007;319(1–2):41-52. https://doi.org/10.1016/j.jim.2006.10.008
16. Ma C, Cheung AF, Chodon T, et al. Multifunctional T-cell analyses to study response and progression in adoptive cell transfer immunotherapy. *Nanosyst Biol Cancer Cent*. 2013;3(4):418-429. https://doi.org/10.1158/2159-8290.CD-12-0383
17. Stacey AJ, Cheeseman EA, Glen KE, Moore RLL, Thomas RJ. Experimentally integrated dynamic modelling for intuitive optimisation of cell based processes and manufacture. *Biochem Eng J*. 2018;132:130-138. https://doi.org/10.1016/j.bej.2018.01.012
18. Glen KE, Cheeseman EA, Stacey AJ, Thomas RJ. A mechanistic model of erythroblast growth inhibition providing a framework for optimisation of cell therapy manufacturing. *Biochem Eng J*. 2018;133:28-38. https://doi.org/10.1016/j.bej.2018.01.033
19. Cost Analysis of Cell Therapy Manufacture: Autologous Cell Therapies, Part 2—BioProcess InternationalBioProcess International. https://bioprocessintl.com/manufacturing/cell-therapies/cost-analysis-of-cell-therapy-manufacturing-autologous-cell-therapies-part-2/. Accessed February 3, 2021.

20. (9) (PDF) Cost analysis of vein-to-vein CAR T-cell therapy: automated manufacturing and supply chain. https://www.researchgate.net/publication/342076749_Cost_analysis_of_vein-to-vein_CAR_T-cell_therapy_automated_manufacturing_and_supply_chain. Accessed February 3, 2021.

21. Future of BioPharma: BioProcess International: Inactivated Poliovirus Vaccine Made in Modular Facilities with Single-Use Technology. http://futurebiopharma.blogspot.com/2014/01/bioprocess-internatonal-inactivated.html. Accessed February 3, 2021.

22. Walther J, Godawat R, Hwang C, Abe Y, Sinclair A, Konstantinov K. The business impact of an integrated continuous biomanufacturing platform for recombinant protein production. *J Biotechnol*. 2015;213: 3-12. https://doi.org/10.1016/j.jbiotec.2015.05.010

23. Glen KE, Workman VL, Ahmed F, Ratcliffe E, Stacey AJ, Thomas RJ. Production of erythrocytes from directly isolated or Delta1 notch ligand expanded CD34+ hematopoietic progenitor cells: process characterization, monitoring and implications for manufacture. *Cytotherapy*. 2013;15(9):1106-1117. https://doi.org/10.1016/j.jcyt.2013.04.008

24. Torres-Acosta MA, Harrison RP, Csaszar E, Rito-Palomares M, Brunck MEG. Ex vivo manufactured neutrophils for treatment of neutropenia-a process economic evaluation. *Front Med*. 2019;6:21. https://doi.org/10.3389/fmed.2019.00021

25. Cameau E, Pedregal A, Glover C. Cost modelling comparison of adherent multi-trays with suspension and fixed-bed bioreactors for the manufacturing of gene therapy products. *Cell Gene Ther Insights*. 2019;5(11):1663-1675.

26. Analysis of Cost of Cell Therapy Manufacturing: Autologous Cell Therapies, Part 1 BioProcess International. https://bioprocessintl.com/manufacturing/cell-therapies/analysis-cost-of-cell-therapy-manufacturing-autologous-cell-therapies-part-1/. Accessed February 3, 2021.

27. Frauwirth KA, Thompson CB. Regulation of T lymphocyte metabolism. *J Immunol*. 2004;172(8):4661-4665. https://doi.org/10.4049/jimmunol.172.8.4661

28. Yu Q, Erman B, Bhandoola A, Sharrow SO, Singer A. In vitro evidence that cytokine receptor signals are required for differentiation of double positive thymocytes into functionally mature CD8+ T cells. *J Exp Med*. 2003;197(4):475-487. https://doi.org/10.1084/jem.20021765

29. Di Dedda C, Vignali D, Piemonti L, Monti P. Preinfusion polyfunctional anti-CD19 chimeric antigen receptor T cells are associated with clinical outcomes in NHL. *Int J Mol Sci*. 2019;20(19):804-814. https://doi.org/10.3390/ijms20194962

30. Swainson L, Kinet S, Manel N, Battini JL, Sitbon M, Taylor N. Glucose transporter 1 expression identifies a population of cycling CD4+CD8+ human thymocytes with high CXCR4-induced chemotaxis. *Proc Natl Acad Sci U S A*. 2005;102(36):12867-12872. https://doi.org/10.1073/pnas.0503603102

31. Palmer CS, Hussain T, Duette G, et al. Regulators of glucose metabolism in CD4+and CD8+T cells. *Int Rev Immunol*. 2016;35(6):477-488. https://doi.org/10.3109/08830185.2015.1082178

32. Sugiura A, Rathmell JC. Metabolic barriers to T cell function in tumors. *J Immunol*. 2018;200(2):400-407. https://doi.org/10.4049/jimmunol.1701041

33. Chakrabarti R, Jung CY, Lee TP, Liu H, Mookerjee BK. Changes in glucose transport and transporter isoforms during the activation of human peripheral blood lymphocytes by phytohemagglutinin. *J Immunol*. 1994;152(6):2660-2668. http://www.ncbi.nlm.nih.gov/pubmed/8144874 Accessed January 10, 2020.

34. Kedia-Mehta N, Finlay DK. Competition for nutrients and its role in controlling immune responses. *Nat Commun*. 2019;10(1):2123. https://doi.org/10.1038/s41467-019-10015-4

35. Menk AV, Scharping NE, Moreci RS, et al. Early TCR signaling induces rapid aerobic glycolysis enabling distinct acute T cell effector functions. *Cell Rep*. 2018;22(6):1509-1521. https://doi.org/10.1016/j.celrep.2018.01.040

36. Jacobs SR, Herman CE, MacIver NJ, et al. Glucose uptake is limiting in T cell activation and requires CD28-mediated Akt-dependent and independent pathways. *J Immunol*. 2008;180(7):4476-4486. https://doi.org/10.4049/jimmunol.180.7.4476

37. Palmer CS, Ostrowski M, Gouillou M, et al. Increased glucose metabolic activity is associated with CD4+ T-cell activation and depletion during chronic HIV infection. *AIDS*. 2014;28(3):297-309. https://doi.org/10.1097/QAD.0000000000000128

38. Dimeloe S, Burgener AV, Grählert J, Hess C. T-cell metabolism governing activation, proliferation and differentiation; a modular view. *Immunology*. 2017;150(1):35-44. https://doi.org/10.1111/imm.12655

39. Cao Y, Rathmell JC, Macintyre AN. Metabolic reprogramming towards aerobic glycolysis correlates with greater proliferative ability and resistance to metabolic inhibition in CD8 versus CD4 T cells. *PLoS One*. 2014;9(8):e104104. https://doi.org/10.1371/journal.pone.0104104

40. Walls J, Sinclair L, Finlay D. Nutrient sensing, signal transduction and immune responses. *Semin Immunol*. 2016;28(5):396-407. https://doi.org/10.1016/j.smim.2016.09.001

41. Betts MR, Brenchley JM, Price DA, et al. Sensitive and viable identification of antigen-specific CD8+ T cells by a flow cytometric assay for degranulation. *J Immunol Methods*. 2003;281(1–2):65-78. https://doi.org/10.1016/S0022-1759(03)00265-5

42. Wanjalla CN, McDonnell WJ, Barnett L, et al. Adipose tissue in persons with HIV is enriched for CD4+ T effector memory and T effector memory RA+ cells, which show higher CD69 expression and CD57, CX3CR1, GPR56 co-expression with increasing glucose intolerance. *Front Immunol*. 2019;10(MAR):408-425. https://doi.org/10.3389/fimmu.2019.00408

43. Kaech SM, Cui W. Transcriptional control of effector and memory CD8+ T cell differentiation. *Nat Rev Immunol*. 2012;12(11):749-761. https://doi.org/10.1038/nri3307

44. Pollard D, Brower M, Abe Y, Lopes AG, Sinclair A. *Standardized Economic Cost Modeling for Next-Generation MAb Production*. Vol 14, Bioprocess International; 2016.

## SUPPORTING INFORMATION

Additional supporting information may be found in the online version of the article at the publisher's website.

Author/s:
Shariatzadeh, M; Lopes, AG; Glen, KE; Sinclair, A; Thomas, RJ

Title:
Application of a simple unstructured kinetic and cost of goods models to support T-cell therapy manufacture.

Date:
2021-08-28

Citation:
Shariatzadeh, M., Lopes, A. G., Glen, K. E., Sinclair, A. & Thomas, R. J. (2021). Application of a simple unstructured kinetic and cost of goods models to support T-cell therapy manufacture.. Biotechnol Prog, pp.e3205-. https://doi.org/10.1002/btpr.3205.

Persistent Link:
http://hdl.handle.net/11343/289743

File Description:
Published version
License:
CC BY